Desalination 496 (2020) 114762

Contents lists available at ScienceDirect

Desalination

journal homepage: www.elsevier.com/locate/desal

Sulfonated nickel phthalocyanine redox flow cell for high-performance electrochemical water desalination

Yanbo Pan, Libo Yao, Dezhen Wu, Abdulaziz Bentalib, Jialu Li, Zhenmeng Peng*

Department of Chemical, Biomolecular and Corrosion Engineering, The University of Akron, Akron, OH 44325, USA

GRAPHICAL ABSTRACT

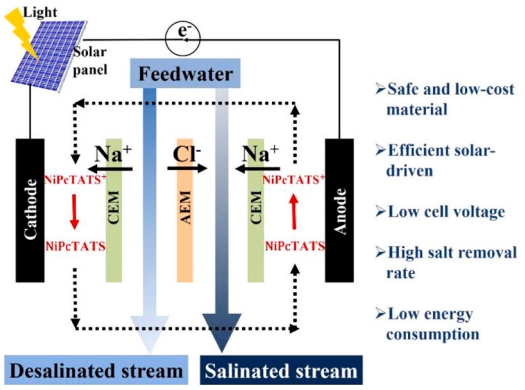

ARTICLE INFO

Keywords:
Water desalination
Redox couple
Metal phthalocyanine
Solar-driven cell

ABSTRACT

With clean water availability raising a great technological and social challenge, saltwater desalination has become a key strategic solution. Herein, we report a nickel phthalocyanine tetrasulfonic acid tetrasodium salt (NiPcTATS)-based redox flow desalination cell (RFDC) that allows safe, efficient and continuous water-salt separation. With the new, water-soluble NiPcTATS/NiPcTATS$^+$ redox couple as electrolyte, the RFDC effectively desalinates saltwater and achieves a high average salt removal rate of 3.11 $g_{NaCl}/(mol_{NiPcTATS}·h)$ and a low energy consumption of 15.0 kJ/mol_{NaCl} at 0.5 V cell voltage. The cell exhibits excellent reversibility and durability for long-term operation, benefiting from the fast-redox kinetics and chemical stability of the redox couple. Efficient solar-driven RFDC for water desalination is demonstrated by powering the cell with a solar panel. This RFDC method provides a low-cost, efficient and safe strategy to purify saltwater, and the findings with NiPcTATS-based redox couple offer new opportunities of utilizing metal phthalocyanines and derivatives in water desalination research.

1. Introduction

Freshwater scarcity has become a critical issue in the past decades due to the increasing world population and expansion of industries and irrigated agriculture, which would greatly threaten over two-thirds of the people worldwide by the year 2025 [1]. According to the Global Risks 2015 report by the World Economic Forum, one in three people lacks sources of water sanitation nowadays, causing over 3.5 million deaths every year. A reliable clean water supply is now one of the most important and challenging issues for the human society [2]. Despite the

* Corresponding author.
E-mail address: zpeng@uakron.edu (Z. Peng).

https://doi.org/10.1016/j.desal.2020.114762
Received 14 May 2020; Received in revised form 9 September 2020; Accepted 10 September 2020
Available online 23 September 2020
0011-9164/ © 2020 Elsevier B.V. All rights reserved.

fact that around 70% of the earth is covered by water, however, 98% of the water on earth is saltwater, with 1.6% of the water being constrained in the polar caps and glaciers and only a very tiny amount (0.4%) of the water being readily drinkable [3].

Over the years, the desalination of saltwater (brackish or seawater) was developed and has become a key strategic solution to satisfy the increasing global water demand. To date, different technologies such as thermal distillation, including multi-stage flash (MSF) [4] and multi-effect distillation (MED) [5], reverse osmosis membrane desalination (RO) [6], electrodialysis (ED) [7,8] and capacitive desalination (CDI) [9] have been developed for clean water production, among which the seawater RO is state-of-the-art technology and has been widely applied in the industries [10]. In a typical seawater RO plant, the clean water production capacity can reach 395,000 m^3/day [11] and the energy consumption can be lowered to the order of 3.5 kWh/m^3 (corresponds to 25 kJ/mol salt) [12] benefiting from the development of novel high flux selective membranes and system optimizations, which is both effective and energy-efficient. However, the shortcomings such as high operation cost and large capital cost of the RO method result in a relatively high clean water production cost, limiting its long-term applications. Other techniques such as MSF and MED require at least one order of magnitude larger energy input than RO [13]. ED and CDI could be more energy-efficient than RO, with the best performance being in the order of 10 kJ/mol salt [14,15]. However, the typical CDI method is primarily based on the mechanism that salt ions in the treated water would be adsorbed to surface of electrode materials, typically carbon-based electrodes, via capacitive adsorption with an applied voltage, resulting in a very limited salt removal capacity of ~1 mg/g to ~40 mg/g salt [16,17]. Battery Electrode Deionization (BDI) that utilizes redox-active electrode materials and associates the desalination process with energy storage, wherein salt ions can be selectively intercalated into lattice of electrode materials along with Faradaic reactions, has attracted an increasing interest in recent years. Diverse systems with different materials or thermodynamic model have been reported so far, such as the $Na_{0.44}MnO_2$-based Na-Ion Desalination (NID) battery [18], the two flow-channel device with porous electrodes containing redox-active nickel hexacyanoferrate (NiHCF) nanoparticles [19], ion-exchange-membrane-free asymmetric CDI by pairing a metal organic framework (MOF) [20], the desalination battery that uses $Cu_3[Fe(CN)_6]_2$ as a Na-storage electrode and Bi as a Cl-storage electrode [21], and the thermodynamic cycle analysis of ICDI (intercalation CDI) to describe the chemical equilibrium between the intercalation electrode and its contacting solution [22]. The BDI mechanism allows a high salt removal capacity, with ~170 mg/g salt removal capacity being reported using a $NaTi_2(PO_4)_3$-based electrode [23]. However, the research in this field has just begun and has mainly achieved progress in electrode materials for sodium ion removal, with only a few successes on electrode materials for chloride ion removal, including sliver [24], bismuth [25], and polypyrrole [26]. Nevertheless, the BDI method would still require big amounts of electrode materials for large scale application [27]. Consequently, cost-intensive techniques such as RO and thermal distillation remain the dominating methods in industrial water desalination.

Very recently, Rivest et al. proposed a new electrochemical desalination mechanism named SUPER (ShUttle-Promoted Electrolyte Removal) [28], in which water-soluble redox couples circulating between anode and cathode are continuously oxidized and reduced to their higher and lower valence states. This would create an imbalance in the charges, which force salt ion migration out of a desalination chamber through ion exchange membrane for charge rebalancing. Compared with BDI, the SUPER method requires a much less amount of redox chemicals, allows continuous operation, and can achieve low operation voltage and energy consumption [28]. In their work, they have reported the selection and study of BTMAP-Fc (1,1′-bis[3-(trimethylammonio)-propyl]ferrocene dichloride) as redox shuttles, with drinkable water production and decent specific energy consumption being demonstrated. This type of redox flow system allows continuous and efficient removal of salt from brine water with low energy consumptions, and thus receives extensive interests in the past few years. For instance, Lee et al. confined the redox reactions of iodide in carbon nanopores in a Faradaic deionization cell that achieved a high water production rate (25 L m^{-2} h^{-1}) and low energy consumption (1.63 Wh L^{-1}) [29]. Kim et al. realized an enhanced salt adsorption capacity (67.8 mg/g) via the redox couple reaction of ferricyanide and ferrocyanide in a multichannel capacitive deionization cell [30]. Nam et al. developed a tandem electrodialysis desalination system using the redox couples of TEMPOL/TEMPOL$^+$ (4-hydroxy-2,2,6,6-tetramethylpiperidine 1-oxyl/oxidized 4-hydroxy-2,2,6,6-tetramethylpiperidine 1-oxyl) that could convert the feedwater (0.6 M NaCl) to 0 and 1.2 M NaCl solutions in the desalination cell and salination cell, respectively [31]. Chen and his collaborators have proposed quite a few redox mediators that can be used in the redox flow desalination systems, such as TEMPOL [32], riboflavin-5′-phosphate sodium salt (FMN-Na) [33], and methyl viologen dichloride ($MVCl_2$) [34], which all achieved good desalination performance and low energy consumption. Although multiple redox couples have been proposed by previous studies, finding more redox couples is still noteworthy but challenging, since the redox couples need to meet some criteria listed in the literature [28]. In other words, the redox couples that are robust, cost-effective and environmentally benign are always desired to achieve energy-efficient and safe clean water production.

Herein we report the use of nickel phthalocyanine tetrasulfonic acid tetrasodium salt (NiPcTATS, chemical structure shown in Fig. S1 in the Supplementary data) based redox flow desalination cell (RFDC) for safe, effective and efficient water-salt separation. Sulfonated metal phthalocyanines represent a family of water-soluble, planar organic molecules, with known characteristics of variable valence states, low toxicity, low cost (although not as low as other materials such as sodium ferrocyanide), excellent thermal and chemical stability, and interesting electronic property [35,36]. The NiPcTATS-based redox couple was prepared by mixing an aqueous solution of NiPcTATS in the pristine form and in an oxidized form (NiPcTATS$^+$) that was produced with an electrochemical method (see Section 2 Materials and methods for details). The fabricated RFDC exhibited a high desalination rate even with a low voltage and as low as about 15.0 kJ/mol salt in energy consumption. Benefiting from no consumption of the redox couple and energy recovery during the salination process, it provides a continuous desalination capability with unlimited salt removal capacity. We also demonstrated the use of simple solar panel for effectively driving the RFDC, proving it a promising and practical technology for clean water production in remote places like islands and ships. These findings prove the effectiveness of NiPcTATS-based redox couples in the redox flow desalination system, which further indicate new opportunities in utilizing the large family of metal phthalocyanine (MPc) and its derivatives for water desalination research.

2. Materials and methods

2.1. Materials

Nickel (II) phthalocyanine-tetrasulfonic acid tetrasodium salt (NiPcTATS) was purchased from Aldrich. Sodium chloride (NaCl) was purchased from Merck kGaA. Anion exchange membrane (AEM, Fumasep FAS-PET-130), cation exchange membrane (CEM, Fumasep FKS-PET-130), and carbon cloth (ELAT, hydrophilic) were from Fuel Cell Store.

2.2. Preparation of the oxidized form of NiPcTATS (NiPcTATS$^+$)

NiPcTATS$^+$ was prepared by one simple electrochemical method utilizing a self-designed redox generation battery cell (Fig. S2 in the Supplementary data). The cell comprises an anode and a cathode,

which comprise a current collector (graphite plate and carbon cloth) and a liquid electrolyte comprising deionized water, 35 mM NiPcTATS (saturated) and 50 mM NaCl. The anode and cathode are separated by two membranes, forming three chambers, which follow the sequence of the anode, Chamber A, anion exchange membrane (AEM), Chamber B, cation exchange membrane (CEM), Chamber C and the cathode. Chamber A and C were filled with the liquid electrolyte, with the peristaltic pumps inducing the electrolyte to circulate from the chamber to its respective electrolyte reservoir. NaCl solution (50 mM) was circulated between Chamber B and the NaCl solution reservoir. With an applied voltage (1.0 V), the electrolyte that contacts the anode (electrolyte in Chamber C) was keeping oxidized, generating the oxidized form of NiPcTATS ($NiPcTATS^+$), while the electrolyte that contacts the cathode (electrolyte in Chamber A) was keeping reduced, generating the reduced form of NiPcTATS. The reactions were kept for 2 h, followed by the collection of the electrolyte in Chamber C that contains mostly $NiPcTATS^+$.

2.3. Preparation of NiPcTATS/$NiPcTATS^+$ redox couple electrolyte

$NiPcTATS/NiPcTATS^+$ (35 mM) redox couple electrolyte was prepared by fully mixing 20 mL of NiPcTATS (35 mM) with 20 mL of the electrolyte in Chamber C that was collected from the above procedure, with a certain amount of NaCl (50 mM) being added to improve the electrical conductivity.

2.4. Electrochemical measurement

The electrochemical measurements were conducted using CHI 760D electrochemical workstation (CH Instruments, Inc.) with a three-electrode system which included a glassy carbon (Ø = 5 mm) as the working electrode, a platinum wire as the counter electrode, and an Ag/AgCl electrode as the reference electrode. The cyclic voltammogram (CV) was conducted in both NiPcTATS (35 mM) solution that contains 50 mM NaCl and the $NiPcTATS/NiPcTATS^+$ (35 mM) redox couple electrolyte at room temperature with a potential sweeping range of −1.2–1.5 V and −0.8–1.5 V, respectively, and a scan rate of 50 mV/s. The CV for the RFDC cell was conducted with the same electrochemical workstation using a two-electrode system and a potential sweeping range of −1.2–1.5 V at a scan rate of 50 mV/s.

2.5. Mechanism of the RFGC

The schematic and mechanism of the RFDC are illustrated in Fig. 1a, with cell structure and photograph of the whole desalination system used in this work being shown in Figs. 1b and S3 in the Supplementary data. The RFDC comprises carbon cloths on graphite plate as cell anode and cathode, and an aqueous electrolyte containing 35 mM $NiPcTATS/NiPcTATS^+$ redox couple and 0.1 M NaCl. The carbon cloth has a thickness of 406 μm, a volumetric density of 0.346 g/cm^3, a porosity of 80% and a carbon content of 99.5%. The anode and cathode are separated by three membranes that form four divided chambers, following a sequence of the cathode, Chamber 1, CEM (cation exchange membrane), Chamber 2, AEM (anion exchange membrane), Chamber 3, CEM, Chamber 4 and the anode (Fig. 1b). The volume of Chamber 1 and Chamber 4 is around 1.0 mL, while the volume of Chamber 2 and Chamber 3 is around 2.7 mL. Due to the typical ion pairing requirement between redox chemicals and neighboring membranes, we utilized a CEM|AEM|CEM configuration to avoid possible permeation of $NiPcTATS/NiPcTATS^+$ through the membranes. The $NiPcTATS/NiPcTATS^+$ electrolyte circulates between the two electrodes (in Chamber 1 and Chamber 4) during operation. With a positive cell voltage, $NiPcTATS^+$ is keeping reduced to NiPcTATS at the cathode and NiPcTATS is keeping oxidized to $NiPcTATS^+$ at the anode. The two electrochemical reactions can be described as:

$$Anode\ (Chamber\ 4):\ NiPcTATS \rightarrow NiPcTATS^+ + e^- \quad (1)$$

$$\text{Cathode (Chamber 1)}:\ NiPcTATS^+ + e^- \rightarrow NiPcTATS \quad (2)$$

This generates extra negative charges and positive charges in electrolyte in Chamber 1 and Chamber 4, respectively. Correspondingly, Na^+ ions are forced to transport through the CEMs from Chamber 2 to Chamber 1 and from Chamber 4 to Chamber 3, and Cl^- ions are forced to transport from Chamber 2 through the AEM to Chamber 3 to restore the charge balance. As a result, both Cl^- and Na^+ ions in Chamber 2 would be continuously removed that leads to clean water production, whereas saltwater in Chamber 3 becomes more concentrated. Because the redox electrolyte circulates between the two electrodes and the $NiPcTATS/NiPcTATS^+$ couple are keeping oxidized and reduced at a same rate, the electrolyte in overall would not be consumed and remain unchanged during operation, which allows a continuous desalination process. The redox reactions at the two electrodes and the ion transport directions would be reversed when a negative cell voltage is applied, which leads to desalination in Chamber 3 stream and salination in Chamber 2 stream. We mainly monitored the conductivity change of Chamber 2 to study the salt removal and recovery in this work since the changes of salt concentrations in Chamber 2 and Chamber 3 are always opposite based on the above discussions. However, we monitored both the conductivities in Chamber 2 and Chamber 3 in some of the desalination experiments for validation of the above discussions. In this regard, all discussions on desalination and salination process in this work refer to the stream in Chamber 2 unless specified otherwise.

2.6. Evaluation of the desalination performance

The desalination test was performed using 40 mL $NiPcTATS/NiPcTATS^+$ (35 mM) electrolyte that was circulated between the electrodes of the RFDC cell in Chamber 1 and Chamber 4 with a flow rate of 25 mL/min. Various concentrations and flow rates of the electrolyte were also used to study their effects on the desalination performance. 50 mM NaCl solution was used as the feed stream and was circulated separately by two peristaltic pumps in Chamber 2 and Chamber 3, with the total volume for each stream being 20 mL and the flow rate being 25 mL/min. The geometric active area of the membranes is 10 cm^2. The voltage was applied and recorded by the CHI 760D electrochemical workstation. The conductivity of the stream in Chamber 2 and Chamber 3 were recorded using a conductivity meter (Mettler Toledo S230 conductivity meter and Inlab 741-ISM conductivity probe). A pH meter (Apera Instruments PC60) was used to monitor the pH change before and after the desalination tests. Some parameters that were used to evaluate the desalination performance were calculated as follows.

The capacity (mAh) was calculated by multiplying the current and time, which can be obtained directly from the electrochemical workstation.

The average salt removal rate ASRR ($g_{NaCl}/(mol_{NiPcTATS}{\cdot}h)$) was calculated as follows:

$$ASRR = \frac{(C - C_0) \times V_{NaCl} \times M_{NaCl}}{C_{electrolyte} \times V_{electrolyte} \times t} \quad (3)$$

The salt removal capacity SRC ($g_{NaCl}/(mol_{NiPcTATS})$) was calculated as follows:

$$SRC = \frac{(C - C_0) \times V_{NaCl} \times M_{NaCl}}{C_{electrolyte} \times V_{electrolyte}} \quad (4)$$

The energy consumption (kJ/mol) was calculated as follows:

$$E = \frac{I \times V \times t}{(C - C_0) \times V_{NaCl}} \quad (5)$$

where C and C_0 is the final and initial concentrations (mol/L) of the stream in Chamber 2, respectively, which could be obtained from the conductivity value and the calibration curve, V_{NaCl} is the total volume

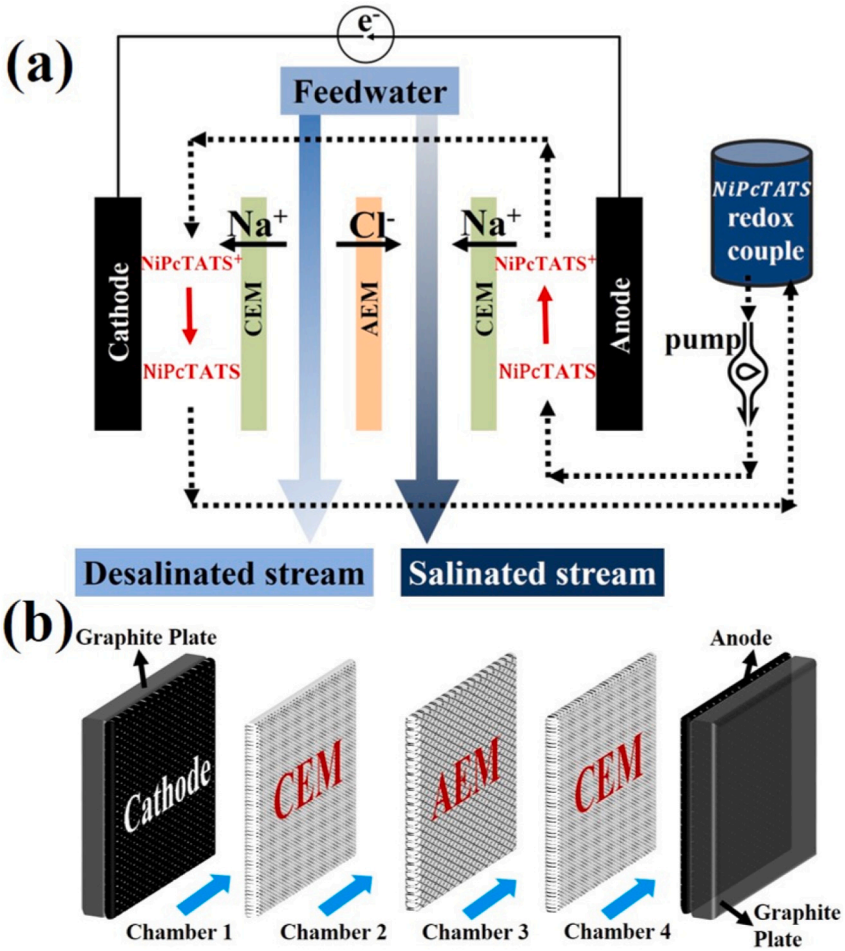

Fig. 1. (a) Schematic and (b) cell structure of the NiPcTATS/NiPcTATS$^+$ redox flow desalination cell (RFDC).

of the stream in Chamber 2 (20 mL), M_{NaCl} is the molar mass of NaCl, $C_{electrolyte}$ and $V_{electrolyte}$ is the molar concentration (mol/L) and total volume of the flow electrolyte, t is the time, I and V is the current and voltage which can be obtained directly from the electrochemical workstation, $I \times V \times t$ is the total energy consumed during the period of interests. When operating at constant cell voltage, $I \times V \times t$ can be obtained by multiplying V and the integrated area of the corresponding I-t plot. When operating at constant current density, $I \times V \times t$ can be obtained by multiplying I and the integrated area of the corresponding V-t plot.

3. Results and discussions

We firstly examined the electrochemical property of pristine NiPcTATS and electrochemically oxidized NiPcTATS using cyclic voltammetry (CV) in a three-electrode system that consisted of a glassy carbon as the working electrode, a platinum wire as the counter electrode and an Ag/AgCl reference electrode. Within the scan range, the pristine NiPcTATS exhibited two oxidation peaks at 0.19 V and 0.92 V and two reduction peaks at −0.01 V and −0.5 V, respectively (Fig. S4 in the Supplementary data). In comparison, the electrochemically oxidized NiPcTATS showed significantly different CV features, with the two oxidation peaks shifting to 0.24 V and 0.81 V and the two reduction peaks shifting to −0.25 V and 0.3 V (Fig. S5). This confirmed electrochemically oxidized NiPcTATS was in a higher valence, which we denoted as NiPcTATS$^+$. Fourier-transform infrared (FTIR) and ultraviolet-visible (UV–vis) spectroscopy characterizations also provided additional evidences for the generated NiPcTATS$^+$. Compared to the pristine NiPcTATS, the NiPcTATS$^+$ possessed new absorbance bands at 1370 cm^{-1} and 1600 cm^{-1} and a much stronger band at 1774 cm^{-1} that were attributed to influences of a higher oxidation state in the molecules to the vibrational spectrum (Fig. S6 in the Supplementary data) [37]. Besides, the NiPcTATS$^+$ exhibited significantly stronger UV–vis absorption than the pristine NiPcTATS in the lower wavelength range (Fig. S7 in the Supplementary data).

By mixing the pristine NiPcTATS and the NiPcTATS$^+$ as electrolyte, multiple redox peaks appeared in pairs on the CV curve that were stable and reversible and suggested a good potential for use in the RFDC (Fig. 2a). We fabricated a RFDC using the NiPcTATS/NiPcTATS$^+$ redox couple mixture electrolyte, with the cell structure illustrated in Fig. 1. 50 mM NaCl solution was used as streams flowing through Chamber 2 and Chamber 3. Fig. 2b shows the CV curve of the whole cell, which was symmetric and tilted in shape and was stable and reversible in electrochemical property [38]. With 0.5 V cell voltage applied for a desalination process in Chamber 2, the current density was initially 1.3 mA/cm^2 and experienced a dramatic decrease to 0.20 mA/cm^2 within the first 150 s, which was attributed to the double layer capacitance effect (Fig. 2c). Upon applying the voltage, the surface of the electrode is charged, attracting the oppositely charged ions to the surface to form an electrical double layer, which generates a large initial current [39]. As this process continues, the surface charge of the electrode is gradually balanced in a very short time, leading to the dramatic decrease of the current. After the current density decrease in Fig. 2c, the value kept almost constant throughout the remaining test, implying a steady-state desalination process. The desalination capacity, which was defined as accumulative charge transfers during the desalination process, showed a nearly linear correlation with time, suggesting a good capability of the RFDC for continuous desalination. Similar

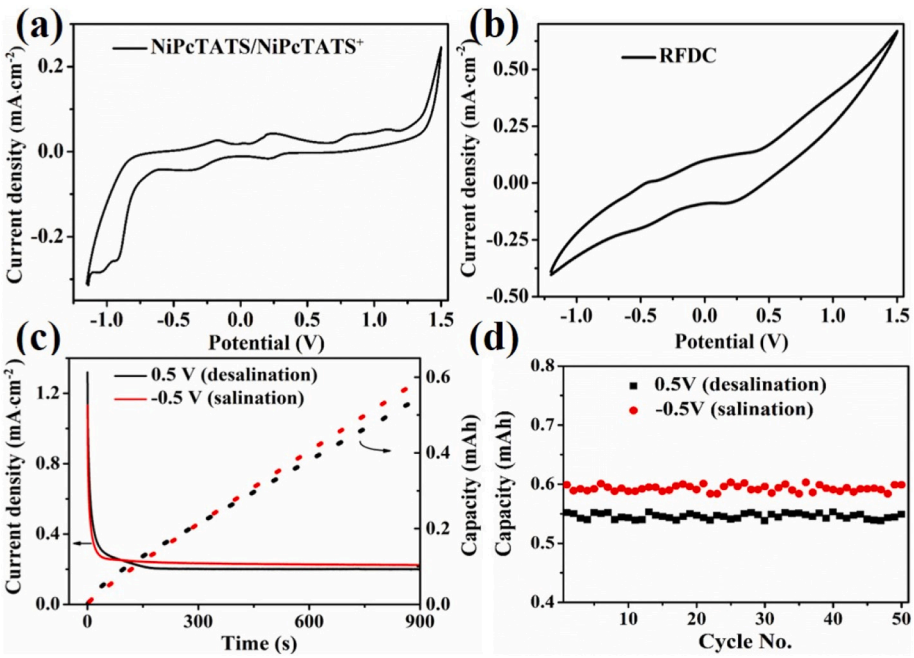

Fig. 2. (a) CV curve of the NiPcTATS/NiPcTATS$^+$ (35 mM) redox couple with a scan rate of 50 mV/s, (b) CV curve of the NiPcTATS/NiPcTATS$^+$ based RFDC with a scan rate of 50 mV/s, (c) measured cell current density and desalination/salination capacity as function of time, and (d) changes in desalination and salination capacity with repeating cycles.

observations were found when −0.5 V cell voltage was applied for a salination process. It was noticed that the obtained salination capacity-time plot was slightly steeper than that for desalination, which could be due to a higher current density in the first few seconds of the salination process as a result of a larger salt concentration gradient between different chambers after the desalination process [40]. With the desalination and salination experiments being repeated for 50 times, the achieved desalination and salination capacities showed very small variations (Fig. 2d), which suggests an excellent stability of the NiPcTATS/NiPcTATS$^+$ RFDC.

We evaluated the salt removal performance of the RFGC by monitoring the conductivity change in the saltwater stream going through Chamber 2 during the desalination (0.5 V) and salination (−0.5 V) processes (Fig. 3a). With 0.5 V cell voltage, the conductivity decreased continuously with time, from an initial 5470 μs/cm to 5350 μs/cm at 900 s, representing effective desalination. During the reverse voltage at −0.5 V, the conductivity recovered gradually to about the initial value within a same length of time. Moreover, the changes in conductivity appeared to be close in repeated desalination and salination experiments for 50 cycles, suggesting a good cyclability and stability of this cell in salt removal and recovering. To translate the conductivity change to the amount of salt removed or recovered, we conducted calibration experiments that built a linear correlation between the concentration of NaCl solution (C_{NaCl}) and the conductivity (Fig. S8). As

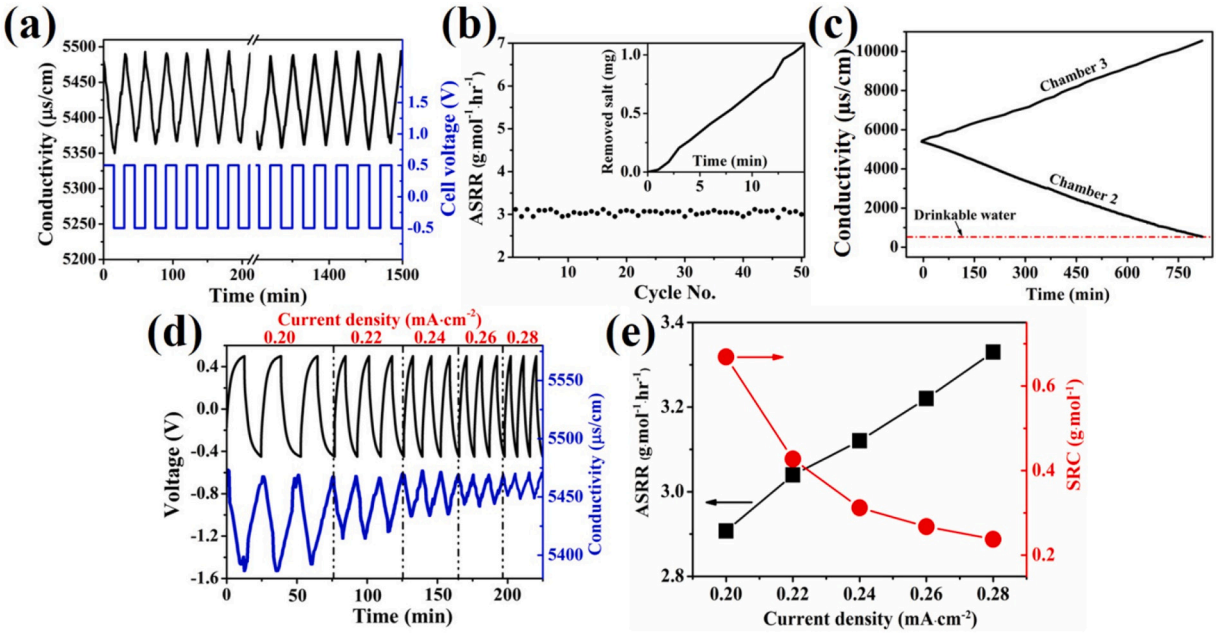

Fig. 3. Desalination performance of the RFDC. (a) The conductivity change with time during cell desalination (0.5 V) and salination (−0.5 V) for 50 cycles, (b) the determined average salt removal rate (ASRR) in different cycles with the inlet showing removed salt amount-time plot for the 1st cycle, (c) the conductivity change in both Chamber 2 and Chamber 3 in the long-term test under 0.5 V, (d) the voltage-time and conductivity-time profiles at different current density, and (e) the influences of current density on ASRR and salt removal capacity (SRC).

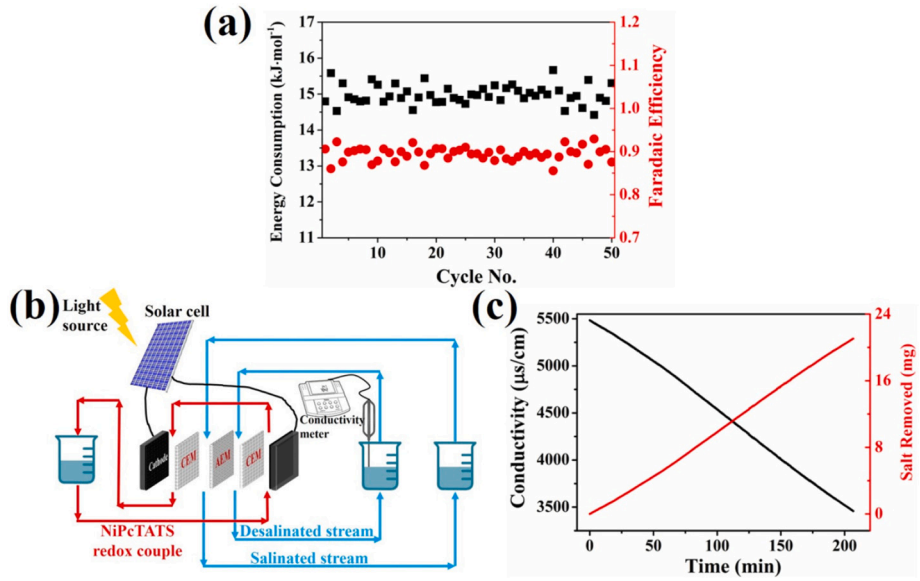

Fig. 4. (a) Energy consumption and Faradaic efficiency in different cycles, (b) schematic of a RFDC system driven by a 1.5 V solar cell, and (c) changes in conductivity and salt removal amount with time in the solar cell-driven RFDC system.

shown in Fig. 3b inlet, the removed salt amount was proportional to the desalination time. We calculated the average salt removal rate (ASRR) in the first desalination process to be 3.11 $g_{NaCl}/(mol_{NiPcTATS}·h)$, which was significantly higher than previous studies and confirmed effectiveness of the cell for desalination [41]. The ASRR ranged from 2.93 to 3.11 $g_{NaCl}/(mol_{NiPcTATS}·h)$ within 50 cycles, reflective of excellent cell stability. To further study the desalination performance and the ion balance in Chamber 2 and Chamber 3 of our RFGC, we conducted a long-term desalination test for about 800 min by monitoring the conductivity in both Chamber 2 and Chamber 3 with a cell voltage of 0.5 V (Fig. 3c). The conductivity in Chamber 2 decreased continuously with time, and reached below the value of drinkable water to around 500 μs/cm within 800 min. As a comparison, the conductivity in Chamber 3 increased almost linearly to a very high level (around 10,000 μs/cm) after the test, indicating that the salt was transferred from Chamber 2 to Chamber 3. The amount of salt removed from Chamber 2 was found to be very close to the amount of salt transferred into Chamber 3 along the time (Fig. S9), suggesting an excellent ion balance in different chambers. These results further validate the working mechanism of our RFDC system. The ASRR for this long-term test was calculated to be 2.80 $g_{NaCl}/(mol_{NiPcTATS}·h)$, which is lower than the cycling tests (3.11 $g_{NaCl}/(mol_{NiPcTATS}·h)$). This can be attributed to the increased systematic resistance during the desalination process in the later stage of the long-term test. It needs mentioned that the redox couple reservoir was left in the air without any inert gas protection during all the long-term and cycling tests, validating the stability of the NiPcTATS/$NiPcTATS^+$ redox couple. We measured the NiPcTATS/$NiPcTATS^+$ content in the water stream in Chamber 2 after the experiments, which contained barely any Ni-containing species with inductively coupled plasma-optical emission spectrometry (ICP-OES) analyses, which indicated no crossover of the NiPcTATS/$NiPcTATS^+$ redox couple into the water stream and confirmed a safe operation for water purification application. The pH value was maintained in the range of 6.5–6.8 in the water stream in Chamber 2 and Chamber 3 during the long-term test, suggesting no presence of any side reactions. We also varied the concentrations and flow rates of the NiPcTATS/$NiPcTATS^+$ redox couple and calculated their corresponding ASRR to study the potential effects of the concentrations and flow rates (Figs. S10 and S11). The ASRR increased proportionally with the concentrations of the redox couple (Fig. S10), from 1.68 $g_{NaCl}/(mol_{NiPcTATS}·h)$ at 15 mM to 3.11 $g_{NaCl}/(mol_{NiPcTATS}·h)$ at 35 mM, benefiting from the faster reaction kinetics of the redox couple at higher concentrations. Dissimilarly, the ASRR firstly increased with flow rate, and then remained almost unchanged (with only a very slight increase) when the flow rate was larger than 25 mL/min. This can be explained by the working mechanism of our RFDC system. When the flow rate of the redox couple is fast enough, the consumed NiPcTATS in Chamber 4 and $NiPcTATS^+$ in Chamber 1 could be complemented by the NiPcTATS/$NiPcTATS^+$ redox couple reservoir in a quick and timely manner, resulting in an almost constant concentration of the redox couple in the cell. In contrast, the concentrations of NiPcTATS in Chamber 4 and $NiPcTATS^+$ in Chamber 1 will be lower than the initial concentrations with slow flow rate, leading to slower reaction kinetics and thus a decreased ASRR. From this perspective, a flow rate of 25 mL/min is fast enough to operate the RFGC effectively.

The influences of current density on the ASRR and salt removal capacity (SRC) were examined by adjusting the current density values during desalination and salination between 0.5 V and −0.5 V, respectively (Fig. 3d). A higher current density resulted in a faster charge (desalination)/discharge (salination) rate but a less charge (desalination)/discharge (salination) capacity, which agrees with previous studies [10]. Correspondingly, this led to an increase in ASRR but a decrease in SRC (Fig. 3d). For instance, at 0.20 mA/cm^2 current density, the ASRR and SRC were determined to 2.87 $g_{NaCl}/(mol_{NiPcTATS}·h)$ and 0.67 $g_{NaCl}/mol_{NiPcTATS}$ at completion of the charge experiment. With a higher 0.28 mA/cm^2, the ASRR increased to 3.33 $g_{NaCl}/(mol_{NiPcTATS}·h)$ whereas the SRC dropped to 0.24 $g_{NaCl}/mol_{NiPcTATS}$. We also adjusted the cell voltage from 0.25 V to 1.0 V and examined the corresponding ASRR, which was found to be proportional with the cell voltage (Fig. S12), benefiting from the larger current density under larger voltage. This indicates the desalination performance of our RFGC could be further improved by applying large cell voltage.

As a critical parameter to evaluate the performance of a desalination cell, the energy consumption was evaluated based on the desalination and salination data. The energy consumption was calculated to be around 15 kJ/mol with small variations in all 50 cycles (Fig. 4a), which is among the best in performance in comparison with most ED, CDI, and other flow battery desalination systems [10,15]. For instance, Kim et al. reported a low energy desalination method using battery electrode deionization that could reach a reduced energy consumption to only 0.02 kWh/kg-NaCl (around 2.0 kJ/mol) [42]. Dai et al. introduced a continuous desalination process based on the redox reaction of a dual

zinc electrode that has an energy consumption of 35.3 kJ/mol [43]. For the SUPER desalination system reported by Beh et al. that has a similar cell architecture with this work, the specific energy consumption can be as low as 0.046 kWh/kg NaCl (around 9.2 kJ/mol) [28]. The energy consumption was found to be proportional to the current density (Table S1 in the Supplementary data), suggesting an even less energy consumption being achievable by further decreasing the current. The Faradaic efficiency (Fig. 4a), also known as the charge efficiency, was introduced to evaluate what percentage of charges have been utilized to remove Na^+ and Cl^- ions in the desalination system. The Faradaic efficiency in this work was calculated as the ratio between the amount of salt being experimentally removed during desalination and the theoretical salt removal amount supposing all charges are utilized for desalination. The obtained Faradaic efficiency remained a high level at around 90% in all 50 cycles (Fig. 4a), suggesting that a vast majority of the charges going through the cell were used to remove salinity. It needs mentioned that a Faradaic efficiency of 90% is among the highest for the redox flow desalination systems, which normally ranges from around 70% to 97% [29,30,33,34]. These results validated the low energy consumption and outstanding Faradaic efficiency of the RFDC.

Given the fact that the NiPcTATS/NiPcTATS$^+$ RFDC can be operated at a low voltage with a low energy consumption, we demonstrated the utilization of a solar panel to directly power it for effective desalination. We connected our RFDC system with a commercially available solar cell panel (AMX3d Mini Solar Cell, 1.5 V, 400 mA) to provide the power supply (Figs. 4b and S13 in the Supplementary data). A solar simulator (PerfectLight PLS-SXE300C) was used for generating light with a comparable intensity with sunlight (137 mW/cm^2). The conductivity decreased nearly linearly with time in this solar-driven RFDC and reached about 3500 μs/cm within about 3.5 h, with the ASRR being determined to be 4.43 $g_{NaCl}/(mol_{NiPcTATS}·h)$ (Fig. 4c). This finding suggests a good potential of integrating the researched NiPcTATS/NiPcTATS$^+$ RFDC with solar cell or other renewable energy sources for practical and sustainable clean water production. Moreover, our RFDC system could be scaled up by simply using electrodes and membranes with larger surface areas, followed by the arrangement of multiple such devices in parallel or in series. It needs noted that this may raise issues such as high operating voltage and large energy consumption due to the large systematic resistance caused by the multi-channel cell structure and connections between different devices [44].

4. Conclusions

To conclude, we developed a novel redox flow desalination cell (RFDC) system using NiPcTATS/NiPcTATS$^+$ redox flow electrolyte that circulates between cell electrodes and is simultaneously oxidized and reduced at the electrodes, which forces salt ions to migrate through ion exchange membranes and drives desalination of saltwater. Benefitting from an excellent redox reversibility of the NiPcTATS/NiPcTATS$^+$ couple, efficient and durable desalination was realized using the fabricated RFDC with cell voltage as low as 0.5 V, with high average salt removal rate (ASRR) of 3.11 $g_{NaCl}/(mol_{NiPcTATS}·h)$ and salt removal rate (SRC) of 0.67 $g_{NaCl}/mol_{NiPcTATS}$ being achieved. The excellent stability of the RFDC was evidenced by small performance variations in the desalination/salination cycle experiments under both constant voltage and constant current density conditions. The energy consumption of the RFDC was determined to be around 15.0 kJ/mol, which was among the lowest compared to the best performed ED, CDI and other redox flow battery in previous studies. Besides, there was no crossover of NiPcTATS and NiPcTATS$^+$ species to the desalinated water stream, proving its safe use for water purification. An integration of the RFDC and a solar cell was demonstrated for effective water desalination driving by solar power, suggesting a good potential in practical circumstances. This work provides a strategy that utilizes cost-effective and environment-friendly NiPcTATS-based redox couples for efficient and safe water desalination. The finding also offers a large family of metal phthalocyanine-based redox couples as new promising candidates to be researched for the water purification application.

CRediT authorship contribution statement

Yanbo Pan: Conceptualization, Investigation, Data curation, Writing original draft. **Libo Yao:** Investigation, Review & editing. **Dezhen Wu:** Investigation, Review & editing. **Abdulaziz Bentalib:** Investigation, Review & editing. **Jialu Li:** Investigation, Review & editing. **Zhenmeng Peng:** Conceptualization, Review & editing, Supervision, Funding acquisition.

Declaration of competing interest

The authors declare that they have no known competing financial interests or personal relationships that could have appeared to influence the work reported in this paper.

Acknowledgment

We acknowledge the financial support of this work by National Science Foundation (CHE-1665265).

Appendix A. Supplementary data

Chemical structure of NiPcTATS, FTIR and UV–vis spectrums, calibration curve between NaCl solution concentrations and conductivity, effects of the concentrations and flow rates of the redox couple, effects of different cell voltage, and photographs of the experimental setup. Supplementary data to this article can be found online at https://doi.org/10.1016/j.desal.2020.114762.

References

[1] M.M. Mekonnen, A.Y. Hoekstra, Four billion people facing severe water scarcity, Sci. Adv. 2 (2) (2016) e1500323.
[2] G. Risks, World economic forum, Insight Report, 10th edition, 2015 Retrived from: http://www3.weforum.org/docs/WEF_Global_Risks_2015_Report15.pdf.
[3] S. Saha, N. Mistry, I. Husein, J. Nilesh, Design and construction of solar water distillation system, Int. J. Sci. Res. Sci. Eng. Technol. 3 (2017) 606–610.
[4] H.T. El-Dessouky, H.M. Ettouney, Y. Al-Roumi, Multi-stage flash desalination: present and future outlook, Chem. Eng. J. 73 (2) (1999) 173–190.
[5] H. Sayyaadi, A. Saffari, Thermoeconomic optimization of multi effect distillation desalination systems, Appl. Energy 87 (4) (2010) 1122–1133.
[6] M. Qasim, M. Badrelzaman, N.N. Darwish, N.A. Darwish, N. Hilal, Reverse osmosis desalination: a state-of-the-art review, Desalination 459 (2019) 59–104.
[7] H.-J. Lee, F. Sarfert, H. Strathmann, S.-H. Moon, Designing of an electrodialysis desalination plant, Desalination 142 (3) (2002) 267–286.
[8] M. Sadrzadeh, T. Mohammadi, Sea water desalination using electrodialysis, Desalination 221 (1–3) (2008) 440–447.
[9] Y. Oren, Capacitive deionization (CDI) for desalination and water treatment—past, present and future (a review), Desalination 228 (1–3) (2008) 10–29.
[10] X. Hou, Q. Liang, X. Hu, Y. Zhou, Q. Ru, F. Chen, S. Hu, Coupling desalination and energy storage with redox flow electrodes, Nanoscale 10 (26) (2018) 12308–12314.
[11] A. Al-Karaghouli, L.L. Kazmerski, Energy consumption and water production cost of conventional and renewable-energy-powered desalination processes, Renew. Sust. Energ. Rev. 24 (2013) 343–356.
[12] J. Imbrogno, J.J. Keating IV, J. Kilduff, G. Belfort, Critical aspects of RO desalination: a combination strategy, Desalination 401 (2017) 68–87.
[13] R. Semiat, Energy issues in desalination processes, Environ. Sci. Technol. 42 (22) (2008) 8193–8201.
[14] B. Pilat, Practice of water desalination by electrodialysis, Desalination 139 (1–3) (2001) 385–392.
[15] W. Zhang, M. Mossad, L. Zou, A study of the long-term operation of capacitive deionisation in inland brackish water desalination, Desalination 320 (2013) 80–85.
[16] S. Porada, R. Zhao, A. Van Der Wal, V. Presser, P. Biesheuvel, Review on the science and technology of water desalination by capacitive deionization, Prog. Mater. Sci. 58 (8) (2013) 1388–1442.
[17] F. Zhou, T. Gao, M. Luo, H. Li, Heterostructured graphene@ $Na_4Ti_9O_20$ nanotubes for asymmetrical capacitive deionization with ultrahigh desalination capacity, Chem. Eng. J. 343 (2018) 8–15.
[18] K.C. Smith, R. Dmello, Na-ion desalination (NID) enabled by Na-blocking membranes and symmetric Na-intercalation: porous-electrode modeling, J. Electrochem. Soc. 163 (3) (2016) A530.
[19] S. Porada, A. Shrivastava, P. Bukowska, P. Biesheuvel, K.C. Smith, Nickel

hexacyanoferrate electrodes for continuous cation intercalation desalination of brackish water, Electrochim. Acta 255 (2017) 369–378.
[20] S. Choi, B. Chang, S. Kim, J. Lee, J. Yoon, J.W. Choi, Battery electrode materials with omnivalent cation storage for fast and charge-efficient ion removal of asymmetric capacitive deionization, Adv. Funct. Mater. 28 (35) (2018) 1802665.
[21] D.-H. Nam, M.A. Lumley, K.-S. Choi, A desalination battery combining $Cu_3[Fe(CN)_6]_2$ as a Na-storage electrode and bi as a Cl-storage electrode enabling membrane-free desalination, Chem. Mater. 31 (4) (2019) 1460–1468.
[22] R. Wang, S. Lin, Thermodynamic reversible cycles of electrochemical desalination with intercalation materials in symmetric and asymmetric configurations, J. Colloid Interf. Sci. 574 (2020) 152–161.
[23] K. Wang, Y. Liu, Z. Ding, Y. Li, T. Lu, L. Pan, Metal–organic-frameworks-derived $NaTi_2(PO_4)_3$/carbon composites for efficient hybrid capacitive deionization, J. Mater. Chem. A 7 (19) (2019) 12126–12133.
[24] M. Pasta, C.D. Wessells, Y. Cui, F. La Mantia, A desalination battery, Nano Lett. 12 (2) (2012) 839–843.
[25] D.-H. Nam, K.-S. Choi, Bismuth as a new chloride-storage electrode enabling the construction of a practical high capacity desalination battery, J. Am. Chem. Soc. 139 (32) (2017) 11055–11063.
[26] H. Kong, M. Yang, Y. Miao, X. Zhao, Polypyrrole as a novel chloride-storage electrode for seawater desalination, Energy Technol. 7 (11) (2019) 1900835.
[27] M.E. Suss, V. Presser, Water desalination with energy storage electrode materials, Joule 2 (1) (2018) 10–15.
[28] E.S. Beh, M.A. Benedict, D. Desai, J.B. Rivest, A redox-shuttled electrochemical method for energy-efficient separation of salt from water, ACS Sustain. Chem. Eng. 7 (15) (2019) 13411–13417.
[29] J. Lee, P. Srimuk, S. Carpier, J. Choi, R.L. Zornitta, C. Kim, M. Aslan, V. Presser, Confined redox reactions of iodide in carbon nanopores for fast and energy-efficient desalination of brackish water and seawater, ChemSusChem 11 (19) (2018) 3460–3472.
[30] N. Kim, S.P. Hong, J. Lee, C. Kim, J. Yoon, High-desalination performance via redox couple reaction in the multichannel capacitive deionization system, ACS Sustain. Chem. Eng. 7 (19) (2019) 16182–16189.
[31] D.-H. Nam, K.-S. Choi, Tandem desalination/salination strategies enabling the use of redox couples for efficient and sustainable electrochemical desalination, ACS Appl. Mater. Inter. 11 (42) (2019) 38641–38647.
[32] J. Wang, Q. Zhang, F. Chen, X. Hou, Z. Tang, Y. Shi, P. Liang, Y. Denis, Q. He, L.-J. Li, Continuous desalination with a metal-free redox-mediator, J. Mater. Chem. A 7 (23) (2019) 13941–13947.
[33] Q. Zhang, S.H. Aung, T.Z. Oo, F. Chen, Continuous electrochemical deionization by utilizing the catalytic redox effect of environmentally friendly riboflavin-5′-phosphate sodium, Mater. Today Commun. 23 (2020) 100921.
[34] F. Chen, J. Wang, Q. Ru, S.H. Aung, T.Z. Oo, B. Chu, Continuous electrochemical desalination via a viologen redox flow reaction, J. Electrochem. Soc. 167 (8) (2020) 083503.
[35] K.N. Unni, C. Menon, Electrical, optical and structural studies on nickel phthalocyanine thin films, Mater. Lett. 45 (6) (2000) 326–330.
[36] G. McHale, M. Newton, P. Hooper, M. Willis, Nickel phthalocyanine photovoltaic devices, Opt. Mater. 6 (1–2) (1996) 89–92.
[37] P. Toman, S. Nešpůrek, K. Yakushi, Electronic states and infrared spectroscopy of Ni-and Co-phthalocyanines: neutral and oxidized forms, J. Porphyr. Phthalocya. 6 (09) (2002) 556–562.
[38] L. Zou, L. Li, H. Song, G. Morris, Using mesoporous carbon electrodes for brackish water desalination, Water Res. 42 (8–9) (2008) 2340–2348.
[39] P. Biesheuvel, M. Bazant, Nonlinear dynamics of capacitive charging and desalination by porous electrodes, Phys. Rev. E 81 (3) (2010) 031502.
[40] H. Pradhan, M. Ghangrekar, Organic matter and dissolved salts removal in a microbial desalination cell with different orientation of ion exchange membranes, Desalin. Water Treat. 54 (6) (2015) 1568–1576.
[41] J. Ma, C. He, D. He, C. Zhang, T.D. Waite, Analysis of capacitive and electrodialytic contributions to water desalination by flow-electrode CDI, Water Res. 144 (2018) 296–303.
[42] T. Kim, C.A. Gorski, B.E. Logan, Low energy desalination using battery electrode deionization, Environ. Sci. Technol. Lett. 4 (10) (2017) 444–449.
[43] J. Dai, J. Wang, X. Hou, Q. Ru, Q. He, P. Srimuk, V. Presser, F. Chen, Dual-zinc electrode electrochemical desalination, ChemSusChem 13 (10) (2020) 2792.
[44] F. Chen, J. Wang, C. Feng, J. Ma, T.D. Waite, Low energy consumption and mechanism study of redox flow desalination, Chem. Eng. J. (2020) 126111.